Journal of Power Sources 308 (2016) 83–96

Contents lists available at ScienceDirect

Journal of Power Sources

journal homepage: www.elsevier.com/locate/jpowsour

A fault-tolerant voltage measurement method for series connected battery packs

Bing Xia [a, b], Chris Mi [a, *]

[a] Department of Electrical and Computer Engineering, San Diego State University, 5500 Campanile Drive, San Diego, CA 92182, USA
[b] Department of Electrical and Computer Engineering, University of California San Diego, 9500 Gilman Dr., La Jolla, CA 92093, USA

HIGHLIGHTS

- Developed a fault-tolerant voltage measurement method for series battery packs.
- Developed matrix interpretation to demonstrate the viability of the method.
- Developed methods to determine and isolate sensor or cell faults by location.
- Validated the condition for valid sensor topology with proof.
- Modeled and analyzed diagnostic confidence, cost and measurement accuracy.

ARTICLE INFO

Article history:
Received 13 November 2015
Received in revised form
12 January 2016
Accepted 14 January 2016
Available online 28 January 2016

Keywords:
Lithium ion battery
Fault tolerance
Sensors
Voltage measurement
Diagnostics

ABSTRACT

This paper proposes a fault-tolerant voltage measurement method for battery management systems. Instead of measuring the voltage of individual cells, the proposed method measures the voltage sum of multiple battery cells without additional voltage sensors. A matrix interpretation is developed to demonstrate the viability of the proposed sensor topology to distinguish between sensor faults and cell faults. A methodology is introduced to isolate sensor and cell faults by locating abnormal signals. A measurement electronic circuit is proposed to implement the design concept. Simulation and experiment results support the mathematical analysis and validate the feasibility and robustness of the proposed method. In addition, the measurement problem is generalized and the condition for valid sensor topology is discovered. The tuning of design parameters are analyzed based on fault detection reliability and noise levels.

1. Introduction

Lithium ion batteries are widely applied in electric vehicle applications due to their considerable improvements in energy density and power density [1,2]. However, this technology still demands many compromises be made in system level, among which safety is the primary concern [3]. Multiple violent incidents reported all over the world hinder the fast growth of lithium battery in the market place [4–6]. These incidents originates from various causes, but they all result in the worst scenario in which thermal runaway is triggered. Thermal runaway has been identified as a catastrophic failure of lithium battery systems and is typically induced by internal or external physical damage of the cell [7]. The initial temperature-rise from a failure cell triggers the exothermic chemical reaction that propagates the temperature-rise among battery packs and eventually lead to fire [8]. According to the post-accident reports, most of the incidents can be avoided or at least mitigated with proper and reliable management [4], which is also believed to be the key to the comprehensive development of lithium ion battery technology [9].

The management of onboard lithium ion batteries gives rise to battery management systems (BMS) [9,10]. The most fundamental task for a BMS is to ensure the safe working condition of batteries by monitoring voltage, current and temperature values [11]. Among all these measurements, research shows that voltage is the most critical information because of its high sensitivity to common electrical faults: including short circuits, over charge and over discharge [12,13]. Thus, it is necessary to enhance the safety level of electric vehicles with reliable and fault-tolerant voltage measurement.

* Corresponding author.
E-mail addresses: bxia@rohan.sdsu.edu (B. Xia), cmi@sdsu.edu (C. Mi).

http://dx.doi.org/10.1016/j.jpowsour.2016.01.057
0378-7753/

Today's widely applied voltage measurement method uses individual voltage sensors, or measurement integrated circuits (ICs), to measure the voltage values of individual cells [14]. This one-to-one correspondence ensures that the voltage of every single cell is monitored. To measure the voltages of a series string of batteries, instead of using one voltage measurement circuit for each of the cells, switches are typically applied to reduce cost in measurement circuits and analog to digital converters (ADC), [15–17]. The switches are turned on with pairs, such that the cell voltages in a string is updated one at a time sequentially. When any voltage reading shows abnormal values, the battery system will be stopped for protection purposes and mitigation methods will be employed.

It needs to be pointed out that sensors have their own reliability; in other words, a voltage sensor in fault condition may lead to a false positive cell fault detection, however, the mitigation methods for these two types of faults differ significantly. In the case of cell faults, some immediate, costly or even dangerous mitigation methods should be taken, including cutting the power from battery pack in the middle of drives and informing the fire department; while in the case of sensor faults, more moderate mitigation methods can be applied, such as switching the vehicle into limp home mode and pushing a request for battery pack maintenance. Thus, it is critical to distinguish between sensor faults and cell faults in order to apply proper mitigation and ensure reliable operation of electric vehicles.

Abundant researches have been conducted to investigate the methods to detect and isolate sensor faults. The most widely applied method is hardware redundancy, where measurements of the same signal are given by multiple sensors [18]. Clearly, this sensor fault detection feature is equipped at the cost of additional hardware expense and more complex system which may be more prone to failure. Analytical redundancy is then proposed as opposed to hardware redundancy, which utilize the output from mathematical models of the system and compare the output with sensor measurements [19]. This method does not require additional hardware, however, it is complex to maintain the robustness of the model given uncertainties, disturbances and various failure modes of the system [20].

Given the inherent disadvantages of the redundancy-based sensor fault diagnostic methods, this paper introduces a fault-tolerant voltage measurement method that can distinguish between a sensor fault and a battery cell fault without any additional sensors. Instead of measuring the voltage values of individual cells, the voltage sensors are used to measure the voltage sum of multiple cells. In this way, a cell voltage value is linked with multiple voltage sensors. When a cell fault occurs, its corresponding voltage sensors will indicate the fault at the same time, thereby identifying the fault.

This paper first provides analysis to sensors with simultaneous measurement. Matrix analysis is used demonstrate the validity of the new measurement topology. Simulation and experiment results prove that the proposed concept can isolate the type and location of a fault robustly.

Then, the proposed method is generalized, which shows the prevailing sensor topology is a special case of this generalization. The reliability prediction analysis is performed to demonstrate the capability of reducing false positive detections. The probability theory is applied to characterize the noise level increase associated with this method.

Next, the impact of sequential measurement to the proposed method is discussed and a procedure is provided to convert sequential measurement to simultaneous measurement in realization. The condition for a valid measurement topology is presented with mathematical proof.

Finally, the tradeoff among different combinations of design parameters are analyzed and discussed in detail.

2. A fault-tolerant design

The drawback of the prevailing voltage measurement method lies in its one-to-one correspondence of voltage sensors and cell voltages, as shown in Fig. 1(a). In real applications, the voltage sensors have their own reliability, and thus a sensor fault may lead to a false positive cell failure detection.

In many industry applications, a second sensor is added to each measurement to provide the redundancy. The data from the second group of sensors will provide validation of the measurement of the first group. Fig. 1(b) shows its embodiment if applied to voltage monitoring for series connected battery packs. The sensors can tell the cell fault in case both sensors give consistent outputs. When the two sensors corresponding to the same cell have different readings, we normally treat it as a sensor fault. However, this method adds significant cost to the system. In particular, the battery packs in electric vehicles consists of hundreds of cells in series. Therefore, the redundancy sensors can add significant cost to the hardware system.

One common solution to this problem is to add a sensor redundancy within a group of measurements, as shown in Fig. 1(c), in which a string voltage sensor is added in addition to the five voltage sensors for the cells. This method improves cell failure detection, but it still cannot distinguish between sensor failure and cell failure when the sensors show inconsistent readings. For example, if the nominal voltage of the five cells in Fig. 1(c) is 3 V, V_1 shows 0 V, V_2 through V_5 show 3 V and V_6 shows 15 V, the fault diagnostic result is different depending on which voltage sensor is trusted. When V_1 is trusted, it indicates C_1 is in external short circuit condition and V_6 is stuck at 15 V due to circuit failure. When V_6 is trusted, it indicates that V_1 is in sensor fault condition and C_1 is in normal condition.

Another voltage measurement topology is illustrated in Fig. 1(d). This topology measures an accurate reference voltage from an IC as the last measurement in one sampling period, which can be used to calibrate sensor offset and detect sensor fault. However, this method requires a precision voltage reference IC for each of the voltage measurement circuit, and it increases the voltage update period by one clock cycle. Except that, this method will always attribute switch/trace malfunction to cell fault.

2.1. Design description

Fig. 1(e) illustrates one embodiment of the proposed fault-tolerant voltage measurement method. In this topology, each voltage sensor measures the voltage sum of two cells, including V_5, which measures the voltage sum of C_1 and C_5. The schematic in Fig. 1(e) ensures that the voltage of each cell is associated with the measurements of two sensors. For example, the voltage value of C_2 is included in the measurements of V_1 and V_2. When C_2 is in external short circuit condition, its terminal voltage drops to zero, and its abnormal voltage value will be revealed by V_1 and V_2 as they both drop from 6 V to 3 V. On the other hand, when a sensor fault occurs, it can be identified immediately in that it is impossible for only one of the sensed voltage values to change. For example, if V_1 through V_5 show 6 V, and suddenly only V_2 changes from 6 V to 0 V, V_2 is certainly in fault condition, otherwise the voltage values of C_1 and C_4 will be 6 V, and C_5's will be 0 V. The latter condition involves the same overcharge level on C_1 and C_4 and an external circuit fault on C_5, which are almost impossible to occur at the same time.

2.2. Matrix interpretation of measurement topologies

The relation between sensor measurements **V** and cell voltage values **C** can be expressed as:

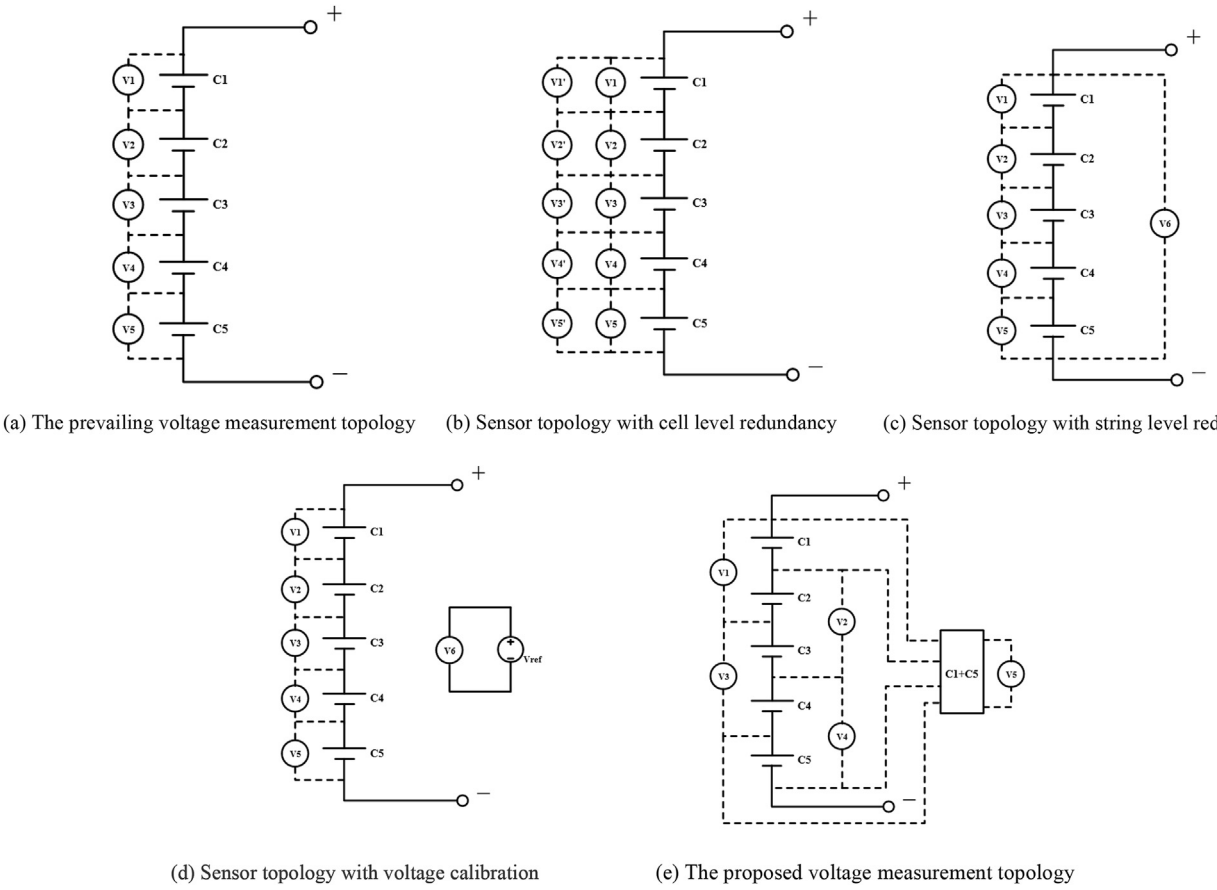

(a) The prevailing voltage measurement topology (b) Sensor topology with cell level redundancy (c) Sensor topology with string level redundancy

(d) Sensor topology with voltage calibration (e) The proposed voltage measurement topology

Fig. 1. Schematics of battery cell voltage sensing.

$$\mathbf{V} = \mathbf{AC} \tag{1}$$

where **V** is an $n \times 1$ matrix that includes all the readings from the voltage sensors, **C** is an $n \times 1$ matrix that includes all the voltage values for the cells in the series connection, and **A** is an $n \times n$ matrix that correlates **V** with **C**.

For the schematics in Fig. 1(a), Eq. (1) can be written as (2). The **A** matrix of (2) demonstrates that each cell voltage corresponds to one voltage sensor. In other words, when a cell fault occurs, only its corresponding voltage sensor can be used to indicate the cell's status. This is also true when the **C** matrix is calculated from the **V** matrix, as shown in (3), in which each sensor reading correlates to only one cell voltage. When a sensor is in fault condition, it is hard to distinguish sensor failure from cell failure.

$$\begin{bmatrix} V_1 \\ V_2 \\ V_3 \\ V_4 \\ V_5 \end{bmatrix} = \begin{bmatrix} 1 & 0 & 0 & 0 & 0 \\ 0 & 1 & 0 & 0 & 0 \\ 0 & 0 & 1 & 0 & 0 \\ 0 & 0 & 0 & 1 & 0 \\ 0 & 0 & 0 & 0 & 1 \end{bmatrix} \begin{bmatrix} C_1 \\ C_2 \\ C_3 \\ C_4 \\ C_5 \end{bmatrix} \tag{2}$$

$$\begin{bmatrix} C_1 \\ C_2 \\ C_3 \\ C_4 \\ C_5 \end{bmatrix} = \begin{bmatrix} 1 & 0 & 0 & 0 & 0 \\ 0 & 1 & 0 & 0 & 0 \\ 0 & 0 & 1 & 0 & 0 \\ 0 & 0 & 0 & 1 & 0 \\ 0 & 0 & 0 & 0 & 1 \end{bmatrix} \begin{bmatrix} V_1 \\ V_2 \\ V_3 \\ V_4 \\ V_5 \end{bmatrix} \tag{3}$$

$$\begin{bmatrix} V_1 \\ V_2 \\ V_3 \\ V_4 \\ V_5 \end{bmatrix} = \begin{bmatrix} 1 & 1 & 0 & 0 & 0 \\ 0 & 1 & 1 & 0 & 0 \\ 0 & 0 & 1 & 1 & 0 \\ 0 & 0 & 0 & 1 & 1 \\ 1 & 0 & 0 & 0 & 1 \end{bmatrix} \begin{bmatrix} C_1 \\ C_2 \\ C_3 \\ C_4 \\ C_5 \end{bmatrix} \tag{4}$$

$$\begin{bmatrix} C_1 \\ C_2 \\ C_3 \\ C_4 \\ C_5 \end{bmatrix} = \begin{bmatrix} \frac{1}{2} & -\frac{1}{2} & \frac{1}{2} & -\frac{1}{2} & \frac{1}{2} \\ \frac{1}{2} & \frac{1}{2} & -\frac{1}{2} & \frac{1}{2} & -\frac{1}{2} \\ -\frac{1}{2} & \frac{1}{2} & \frac{1}{2} & -\frac{1}{2} & \frac{1}{2} \\ \frac{1}{2} & -\frac{1}{2} & \frac{1}{2} & \frac{1}{2} & -\frac{1}{2} \\ -\frac{1}{2} & \frac{1}{2} & -\frac{1}{2} & \frac{1}{2} & \frac{1}{2} \end{bmatrix} \begin{bmatrix} V_1 \\ V_2 \\ V_3 \\ V_4 \\ V_5 \end{bmatrix} \tag{5}$$

The **A** matrix of the proposed method in Fig. 1(e) is shown in (4). By observing the columns of the **A** matrix, it can be found that the voltage value for each cell is linked to two voltage sensors. For example, the two '1's in the third column $[0 \quad 1 \quad 1 \quad 0 \quad 0]^T$ indicate that the voltage value of C_3 is included in both V_2 and V_3. This feature ensures that when cell failure occurs, it will be revealed by two sensors. The probability of two sensors exhibiting the same sensor fault at the same time is a low probability, therefore cell failure can be determined with high confidence. Similarly, $\mathbf{A^{-1}}$ in (5) indicates that when a sensor fault occurs, the abnormal change in the voltage sensor is to be reflected by multiple calculated cell

values. In addition, some of the changes in the cell voltage values are positive to the sensor change and some of the changes in cell voltage values are negative to the sensor change. This feature further increases the sensor fault diagnostic's credibility because simultaneous voltage changes in different directions with the same amplitude at the same time are extremely abnormal in series connected packs.

3. Fault isolation

The fault cell can be located based on the locations of sensors showing abnormal values. If the cell failure is modeled as the sum of normal cell voltages and the effect of fault conditions, it can be expressed as

$$\mathbf{C} = \mathbf{C}_{\mathbf{normal}} + \mathbf{C}_{\mathbf{fault}} \tag{6}$$

where $\mathbf{C}_{\mathbf{normal}}$ is the cell voltage values in normal working condition, and $\mathbf{C}_{\mathbf{fault}}$ is the impact of the fault conditions. $\mathbf{C}_{\mathbf{fault}}$ can be isolated by,

$$\mathbf{C}_{\mathbf{fault}} = \mathbf{C} - \mathbf{C}_{\mathbf{normal}} = \mathbf{A}^{-1}\mathbf{V} - \mathbf{C}_{\mathbf{normal}} \tag{7}$$

where $\mathbf{V}$ is the voltage readings after the fault occurs and $\mathbf{C}_{\mathbf{normal}}$ is the cell voltages in normal conditions. When $\mathbf{C}_{\mathbf{fault}}$ is determined, the indices of cells in fault condition are found and their influence on normal voltage values is also determined.

Likewise, the sensor fault location can be determined according to the indices of cells with abnormal voltage variations. If the sensor failure is modeled as the sum of the sensor reading under normal condition and the effect of fault conditions, it can be expressed as

$$\mathbf{V} = \mathbf{V}_{\mathbf{normal}} + \mathbf{V}_{\mathbf{fault}} \tag{8}$$

where $\mathbf{V}_{\mathbf{normal}}$ is the normal reading and $\mathbf{V}_{\mathbf{fault}}$ is the impact of the fault conditions. $\mathbf{V}_{\mathbf{fault}}$ can be isolated by

$$\mathbf{V}_{\mathbf{fault}} = \mathbf{V} - \mathbf{V}_{\mathbf{normal}} = \mathbf{V} - \mathbf{A}\mathbf{C}_{\mathbf{normal}} \tag{9}$$

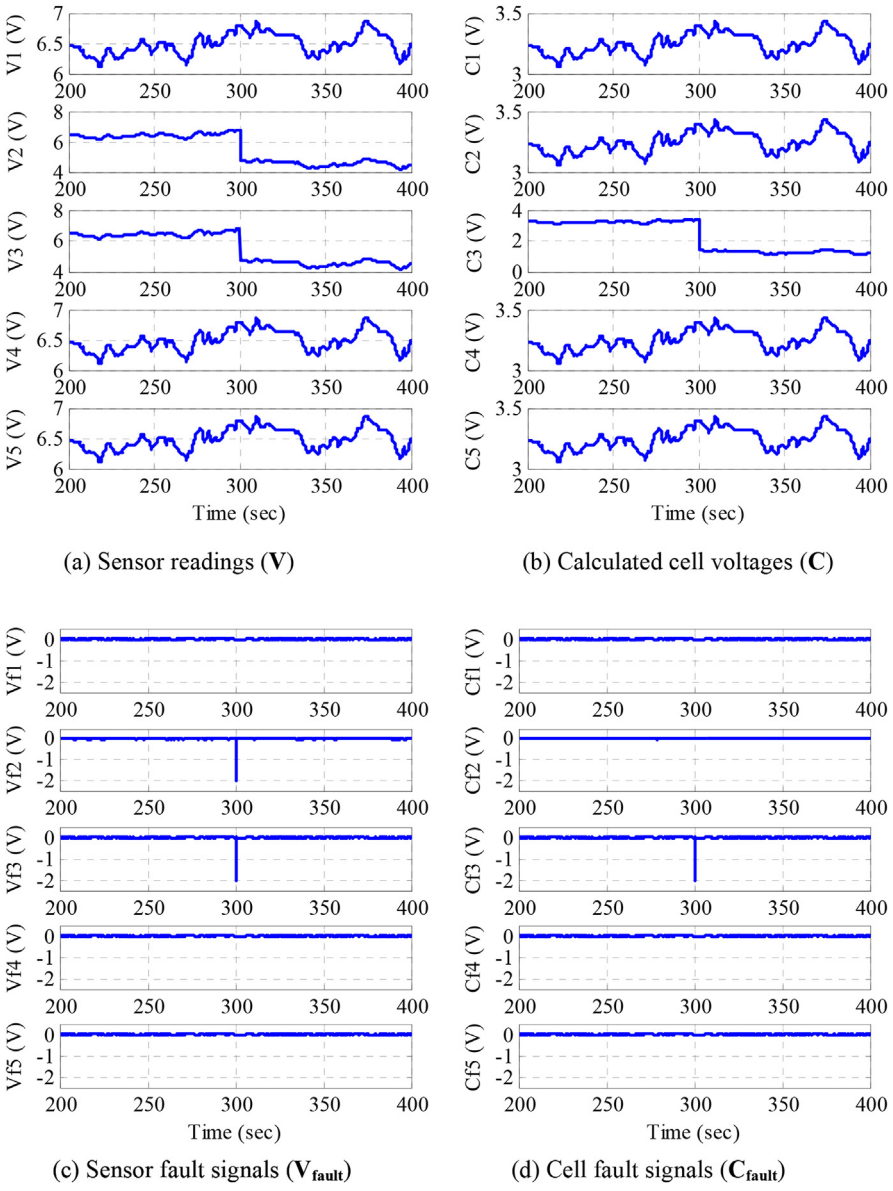

(a) Sensor readings ($\mathbf{V}$)

(b) Calculated cell voltages ($\mathbf{C}$)

(c) Sensor fault signals ($\mathbf{V}_{\mathbf{fault}}$)

(d) Cell fault signals ($\mathbf{C}_{\mathbf{fault}}$)

Fig. 2. External short circuit simulation for C3 at 300 s.

When $\mathbf{V_{fault}}$ is determined, the index of the sensor in fault condition can be found and its influence on normal sensor readings is determined.

4. Simulation

The simulation is set up to test the viability of the proposed fault-tolerant voltage measurement method. A SIMSCPAPE model is built for a battery pack consisting of five battery cells in series connection. In order to demonstrate the robustness of the method in dynamic situation, the urban dynamometer driving schedule (UDDS) cycle is applied to the battery pack when the faults are induced.

An external short circuit fault on C_3 is induced at 300 s by reducing C_3 by 2 V. The simulation results are shown in Fig. 2. It needs to be noted that the reduction in voltage is assigned qualitatively and is only used to demonstrate the viability of the proposed method. At 300 s, the readings of V_2 and V_3 drop by 2 V, indicating a sudden 2 V voltage drop in the overlap of V_2 and V_3. Clearly, C_3 is the overlap and it is demonstrated by the calculated cell terminal voltages.

The same conclusion can be drawn by comparing $\mathbf{V_{fault}}$ and $\mathbf{C_{fault}}$ signals provided in Fig. 2(c) and (d). $\mathbf{V_{fault}}$ indicates that two sensor faults on both V_2 and V_3 at 300 s, while $\mathbf{C_{fault}}$ flags a sudden 2 V voltage drop on C_3. There are two possible explanations: 1) Two sensor faults happen at 300 s and these lead to a wrong voltage calculation on C_3; 2) C_3 is in external circuit fault and this leads to abnormal readings on both V_2 and V_3. Clearly, the latter explanation is more convincing because it is less likely for two sensors to go wrong at the same sampling period.

Similarly, the sensor fault is simulated by setting V_2 to zero after 300 s. The simulation results are shown in Fig. 3. With wrong reading from V_2 after 300 s, the five voltage values all turns abnormal. The offset of the cell voltages follows the trend shown by the second column of (5), which leading the system to flag a sensor fault to V_2 at 300 s, instead of five abnormal cell faults.

5. Experimental

Experiments are set up to demonstrate the concept of the

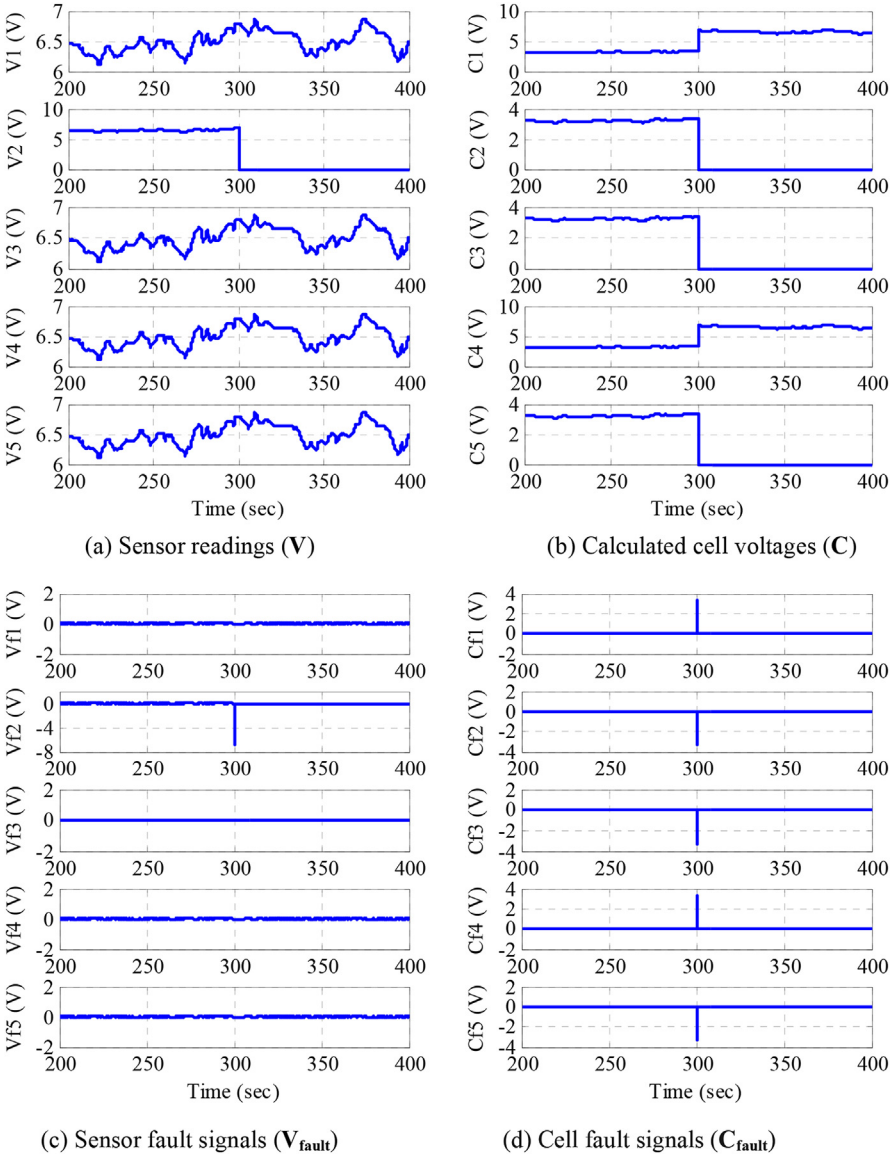

Fig. 3. Sensor fault simulation for V2 at 300 s.

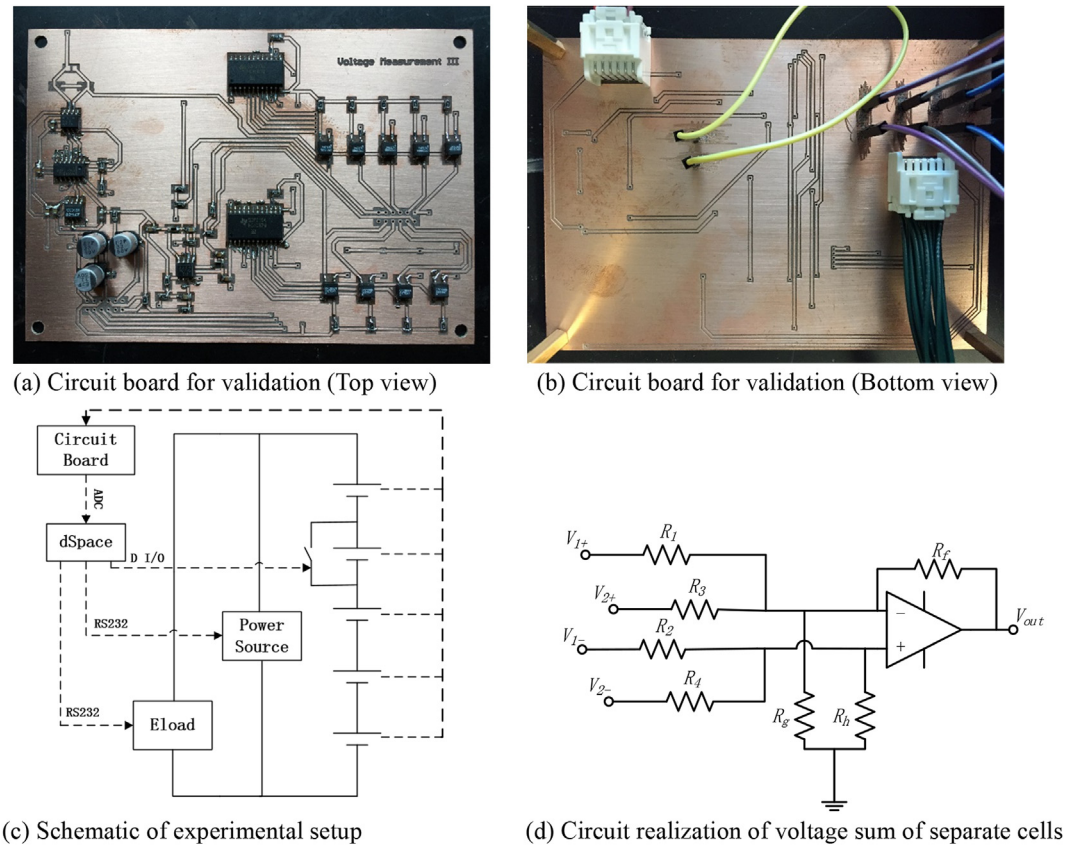

(a) Circuit board for validation (Top view)

(b) Circuit board for validation (Bottom view)

(c) Schematic of experimental setup

(d) Circuit realization of voltage sum of separate cells

Fig. 4. Experimental setup for validation.

proposed method. A circuit board is built based on the diagram in Fig. 1(e), as shown in Fig. 4(a) and (b). The schematic of the experimental setup is shown in Fig. 4(c). The voltage sum of two separate cells in series can be realized in hardware by the circuit given in Fig. 4(d). The positive and negative terminals of the first cell are connected to V_{1+} and V_{1-}. The second separate cell is connected to V_{2+} and V_{2-}. By properly choosing the resistors, i.e., $R = R_1 = R_2 = R_3 = R_4 = R_f$ and $R_h = R_g R/(R_g + R)$, the output will be the inverse of the sum of the two voltage values, i.e. $V_o = -(V_{1+} - V_{1-} + V_{2+} - V_{2-})$. It needs to be noted that the only added cost of the circuit in Fig. 4(d) compared to commercial differential amplifiers is an additional pair of resistors, i.e., R_3 and R_4, which is negligible.

An external short circuit fault is induced by shorting C_2 with a relay. The resistance of the wires and relay is 0.87 Ω. The external short circuit lasts for 1 s and then the relay is opened. Experiment results in Fig. 5(a) show that V_1 and V_2 indicate abnormal voltage changes at 232.8 s and lasting for 1 s. The calculated cell voltage values in Fig. 5(b) demonstrate that C_2 shows abnormal voltage values at 232.8 s lasting for 1 s. In this situation, it is obvious that the probability of two sensors experiencing the same sensor fault at the same time is much lower than that of one cell undergoing an external short circuit. The fault signal in Fig. 5(d) indicates an abnormal voltage drop in C_2. Thus, a cell fault is determined.

The sensor fault is induced by disconnecting the jump wire in the sensing path of V_4 on the bottom side of the circuit board. Experiment results in Fig. 6(b) shows that the calculated cell voltages demonstrate abnormal values at 233.1 s. The voltage values of C_1 and C_3 are increased, while those of C_2, C_4 and C_5 are decreased. These changes are of same magnitude and the signs follows those of the fourth column of (5). As a result, the sensor fault on V_4 is determined.

6. Discussion

6.1. Generalization of the problem

The proposed voltage measurement method can be extended to a battery pack with n cells in series, in which each voltage sensor measures the voltage sum of k cells ($k < n$). It needs to be noted that, given the measurement circuit in Fig. 4(d), the n cells can be nonconsecutive, as demonstrated in (10) and (11), so long as the **A** matrix is invertible. It is interesting to see that the prevailing sensing topology is a special case of this general topology with $k = 1$.

In the previous sections, the case of $n = 5$ and consecutive $k = 2$ is demonstrated. However, the combination of $n = 5$ and $k = 2$ may not be the optimal solution for the battery packs of electric vehicles, whose n may exceed several tens or even hundreds.

In the following section, the choice of n and k values are analyzed in terms of cost, fault detection reliability and noise level increase, and the condition for valid measurement topology is presented.

$$\begin{bmatrix} V_1 \\ V_2 \\ V_3 \\ V_4 \\ V_5 \end{bmatrix} = \begin{bmatrix} 1 & 0 & 1 & 0 & 0 \\ 0 & 1 & 0 & 1 & 0 \\ 0 & 0 & 1 & 0 & 1 \\ 1 & 0 & 0 & 1 & 0 \\ 0 & 1 & 0 & 0 & 1 \end{bmatrix} \begin{bmatrix} C_1 \\ C_2 \\ C_3 \\ C_4 \\ C_5 \end{bmatrix} \tag{10}$$

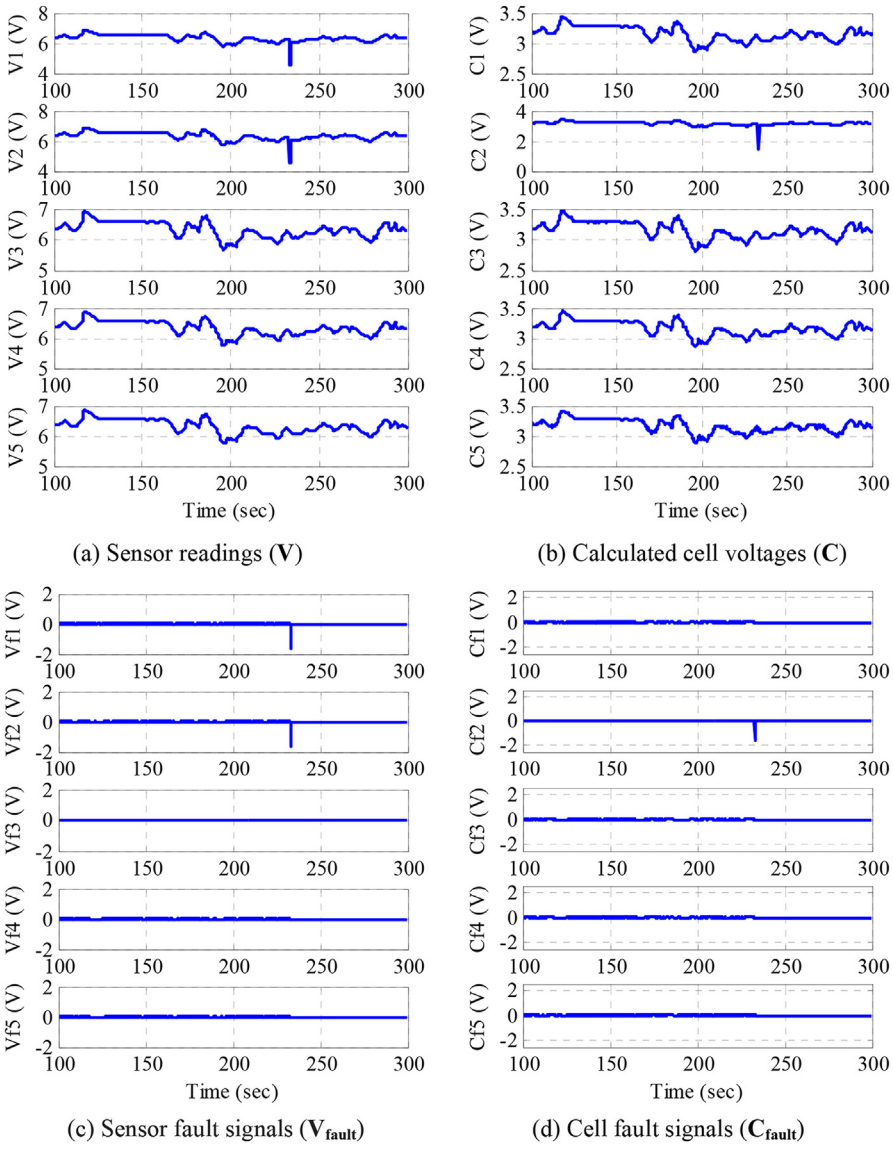

(a) Sensor readings (**V**) (b) Calculated cell voltages (**C**)

(c) Sensor fault signals ($\mathbf{V}_{\mathbf{fault}}$) (d) Cell fault signals ($\mathbf{C}_{\mathbf{fault}}$)

Fig. 5. External short circuit experiment for C2 at 232.8 s.

$$\begin{bmatrix} C_1 \\ C_2 \\ C_3 \\ C_4 \\ C_5 \end{bmatrix} = \begin{bmatrix} \frac{1}{2} & -\frac{1}{2} & -\frac{1}{2} & \frac{1}{2} & \frac{1}{2} \\ \frac{1}{2} & \frac{1}{2} & -\frac{1}{2} & -\frac{1}{2} & \frac{1}{2} \\ \frac{1}{2} & \frac{1}{2} & \frac{1}{2} & -\frac{1}{2} & -\frac{1}{2} \\ -\frac{1}{2} & \frac{1}{2} & \frac{1}{2} & \frac{1}{2} & -\frac{1}{2} \\ -\frac{1}{2} & -\frac{1}{2} & \frac{1}{2} & \frac{1}{2} & \frac{1}{2} \end{bmatrix} \begin{bmatrix} V_1 \\ V_2 \\ V_3 \\ V_4 \\ V_5 \end{bmatrix} \tag{11}$$

6.2. Reliability analysis

The voltage measurement system can be modeled as a series connected system [21], where each voltage sensor is one of the subsystems. Only when all the subsystems are functioning well, the whole system is in normal condition. If any of the subsystems fails, the whole system fails and a fault is flagged.

The reliability of a voltage sensor is modeled as a device with constant failure rate, as shown in

$$R_i(t) = e^{-\lambda t}, \lambda > 0 \tag{12}$$

where R is the reliability of a voltage sensor, λ is the constant failure rate and all the voltage sensors are assumed to have the same failure rate.

When the sensor fault does not occur, the proposed method works the same as traditional one-to-one correspondence measurement topology does. However, when the sensor fault occurs, the traditional method flags a cell fault, but the proposed method flags sensor fault unless all the associated sensors are in fault condition within the same sampling period. The confidence level of the sensor fault detection from the proposed method can be expressed as

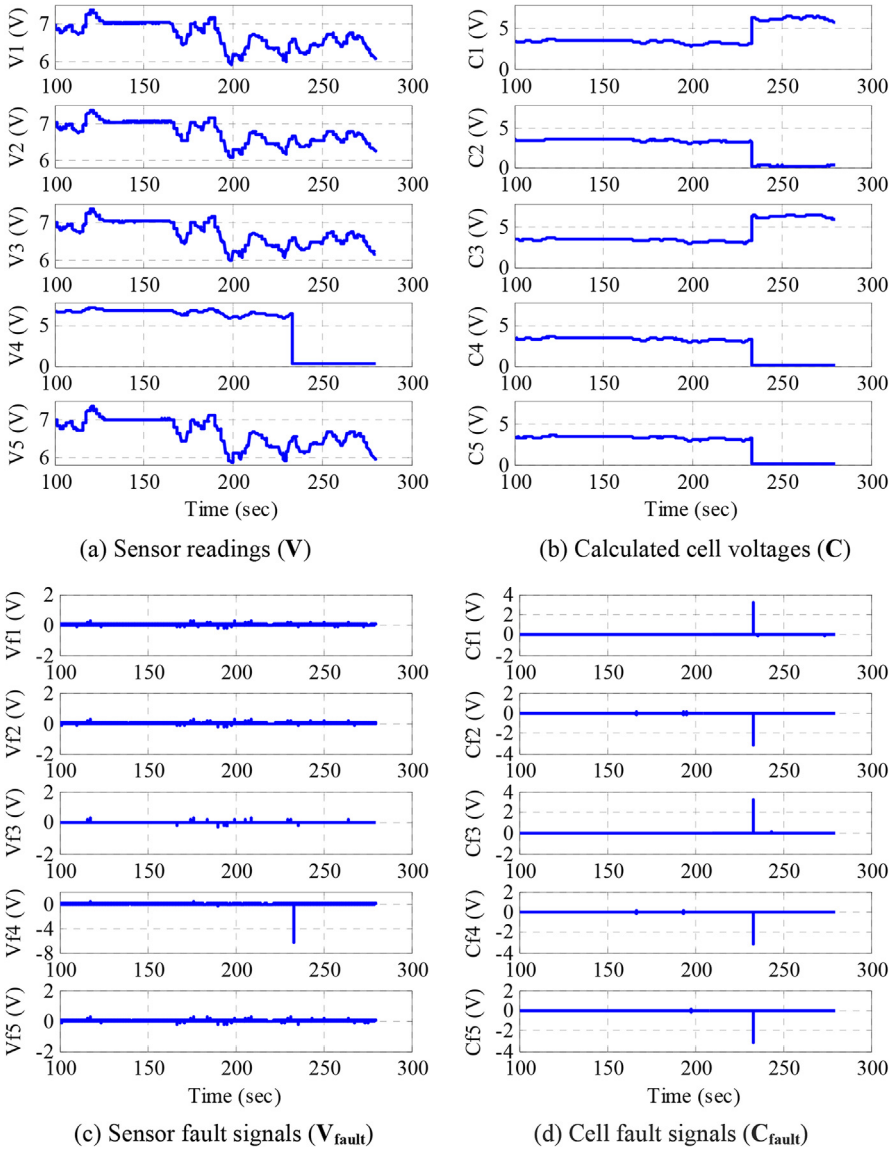

Fig. 6. Sensor fault experiment for V4 at 233.1 s.

$$CL = 1 - P(k\ sensors\ fail|1\ sensor\ fails) = 1 - \frac{\prod_{i=1}^{k}\int_{t=0}^{Ts} f_i(t)dt}{\int_{t=0}^{Ts} f_j(t)dt}$$

$$= 1 - \prod_{i=1}^{k-1}\int_{t=0}^{Ts}\left(1 - e^{-\lambda t}\right)dt \tag{13}$$

where CL is the confidence level of the sensor fault detection ranging from 0 to 1, Ts is the sampling period of the voltage measurements, $f_i(t)$ is the failure density of voltage sensor i, and j is an arbitrary number within 1 and k. The relation between $f_i(t)$ and $R_i(t)$ is given by Ref. [22].

$$R_i(t) + F_i(t) = 1 \tag{14}$$

$$f(t) = \frac{d}{dt}F(t) \tag{15}$$

where $F_i(t)$ is the unreliability of voltage sensor i.

There are two key points that needs to be pointed out from (13),

a) The larger the k is, the more confidence the BMS has in the sensor fault detection. In the traditional voltage measurement topology as shown in Fig. 1(a), k is 1. This leads the CL value drop to zero when the sensor fault occurs, which indicates that the traditional topology gives a false cell fault detection whenever a sensor fault occurs. As for the proposed method, k is larger than 1, which significantly increases the CL value. This is the key to improve the fault detection confidence.

b) The smaller the Ts is, the more confidence in the fault detection. This is due to the monotonic increase of the integral of failure intensity. In practice, it refers to the fact that it is less possible for multiple sensors to fail within a shorter period of time.

The above two points are illustrated in Fig. 7, where the CL values are plotted with different sampling times and different k's. With a fixed k, the detection confidence decreases as Ts increases.

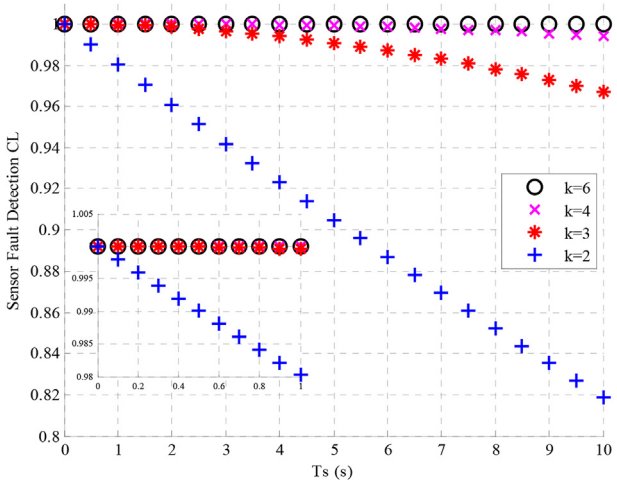

Fig. 7. Fault detection reliability increases as i) k increases ii) Ts decreases. ($\lambda = 0.02$/s).

With a fixed *Ts*, the detection confidence increases as *k* increases. Since the typical sampling period for BMS is smaller than 1 s, the inset in Fig. 7 gives detailed figure for *Ts* smaller than 1 s. The result shows that, when the sensor fault occurs, the proposed method can eliminate more than 98% of the false cell fault detection.

6.3. Noise analysis

If the voltage measurement of a voltage sensor is modeled as a normal distribution with mean value μ and standard deviation σ. The variance of the sensor *i* is denoted as (16). By the variance sum rule [23], shown in (17), the noise levels of the voltage measurements may increase as *k* increases. As the case of (5), the cell voltage values involves the noises from all five voltage sensors.

$$Var(V_i) = \sigma_{V_i}^2 \tag{16}$$

$$Var(aV_i + bV_j) = a^2\sigma_{V_i}^2 + b^2\sigma_{V_j}^2 \tag{17}$$

It is proved in Appendix A that the rows of $\mathbf{A^{-1}}$ matrix rotate one entry to the right as the row number increases by one. This fact indicates that the entries of the rows simply changes their positions when row number changes, as shown in (5), but the sum of square of the entries in each row are the same. If the noise level is regarded as the standard deviation of the measurement [24], and the noise level is assumed to be proportional to the measurement range, the general expression for the noise level of the cell voltages can be expressed as

$$NL = k\sigma\sqrt{\sum_{j=1}^{n} e_{i,j}^2}, \quad \text{for any } i \le n \tag{18}$$

where *NL* represents the noise level of the cell voltage calculation, and σ is the noise level for one of the voltage sensors applied, and $e_{i,j}$ is the *j*th entry in *i*th row of $\mathbf{A^{-1}}$. The noise level gain (G_{NL}) gives the ratio of noise level of the system with (n, k) compared with that of the sensing topology with $k = 1$, and can be expressed as (19). As a special case, $G_{NL} = 1$ when $k = 1$.

$$G_{NL} = k\sqrt{\sum_{j=1}^{n} e_{i,j}^2}, \quad \text{for any } i \le n \tag{19}$$

Since the battery cells are typically treated by the maximum number of 16, the G_{NL} values and their corresponding (n,k) pairs are given in Table 1. It can be concluded from the table that there is no consistent trend for G_{NL} as k or n increases. However, for $n \le 16$: when $k \le 4$, G_{NL} increases as n increases; when $k \le 5$, G_{NL} increases as k value increases. Among all the combinations of n and k, (3, 2) has the lowest G_{NL} and is most favorable in the case of the lowest noise level.

6.4. Extension to sequential measurement

6.4.1. Cost analysis

As introduced in section 1, sequential measurement is utilized to reduce hardware cost. With this measurement method, the number of switches required for *n* cells in series is 2*n* because two switches are needed at a time to deliver voltage signal to the sampling circuit. However, if voltage sum from two nonconsecutive cells is sampled each time, four switches are needed at a time, as shown in Fig. 4(d). In other words, the cost of switches goes up as the number of nonconsecutive cells increases, which is not favorable. Therefore, in the following analysis, only measurement topology with consecutive cells are discussed.

6.4.2. Impact of sequential measurement on the proposed method

The sequential update for the prevailing sensor topology uses zero order hold between samples. An example of $n = 3$ and $k = 2$ is used to demonstrate its principle. If the sequential update is applied to the proposed method, the update formula for C_1 can be expressed as

Table 1
Noise level gain values with different k and n ($n \le 16$).

G_{NL}		*n*													
		3	*4*	*5*	*6*	*7*	*8*	*9*	*10*	*11*	*12*	*13*	*14*	*15*	*16*
k	***2***	1.7		2.2		2.7		3.0		3.3		3.6		3.9	
	3		2.7	3.3		3.6	4.1		4.4	4.8		5.0	5.4		5.6
	4			3.6		4.8		5.0		5.9		6.1		6.9	
	5				4.7	6.6	6.9	6.2		6.4	8.5	8.8	7.7		7.8
	6					5.6				7.7		7.8			
	7						6.6	10.4	10.2	10.3	12.0	9.1		9.2	13.9
	8							7.6		12.8		14.0		10.5	
	9								8.5	14.9		13.7	13.8		17.9
	10									9.5		16.6			
	11										10.5	19.8	19.7	18.8	17.2
	12											11.5			
	13												12.5	25.1	24.1
	14													13.5	
	15														14.5

$$
\begin{aligned}
C_1[m] &= e_{1,1}V_1[m-2] + e_{1,2}V_2[m-1] + e_{1,3}V_3[m] \\
C_1[m+1] &= e_{1,1}V_1[m+1] + e_{1,2}V_2[m-1] + e_{1,3}V_3[m] \\
C_1[m+2] &= e_{1,1}V_1[m+1] + e_{1,2}V_2[m+2] + e_{1,3}V_3[m] \\
C_1[m+3] &= e_{1,1}V_1[m+1] + e_{1,2}V_2[m+2] + e_{1,3}V_3[m+3]
\end{aligned} \tag{20}
$$

where $C_1[m]$ is the voltage value of C_1 at time m, $V_i[m]$ is the updated voltage measurement of sensor i at time m, and $e_{1,1} = 0.5$, $e_{1,2} = -0.5$ and $e_{1,3} = 0.5$ for $n = 3$ and $k = 2$. In this sequential update algorithm, one V_i is updated after every sampling interval, as a result, C_1 is updated after every sampling interval.

A simulation is run based on the update algorithm, where the following assumptions are made.

a) The three batteries are consistent.

b) The terminal voltages of all the batteries jump from 3.0 V to 3.1 V at time $m + 1$.

Base on the simulation, a voltage ripple is observed after the step input, as shown in Fig. 8(a). This voltage ripple can be explained when (20) is rewritten as (21).

$$
\begin{aligned}
C_1[m+1] - C_1[m] &= e_{1,1}\{V_1[m+1] - V_1[m-2]\} \\
C_1[m+2] - C_1[m+1] &= e_{1,2}\{V_2[m+2] - V_2[m-1]\} \\
C_1[m+3] - C_1[m+2] &= e_{1,3}\{V_3[m+3] - V_3[m]\}
\end{aligned} \tag{21}
$$

As can be calculated from (21), from time step m to $m + 1$, C_1 is increased by 0.1 V, from $m + 1$ to $m + 2$, C_1 is decreased by 0.1 V, and from $m + 2$ to $m + 3$, C_1 is increased by 0.1 V. The ripple in Fig. 8(a) results from the latter two changes. Indeed, the effect of the ripple can be larger given larger n and k, as shown in Fig. 8(a), where the case of $n = 5$ and $k = 3$ is also demonstrated.

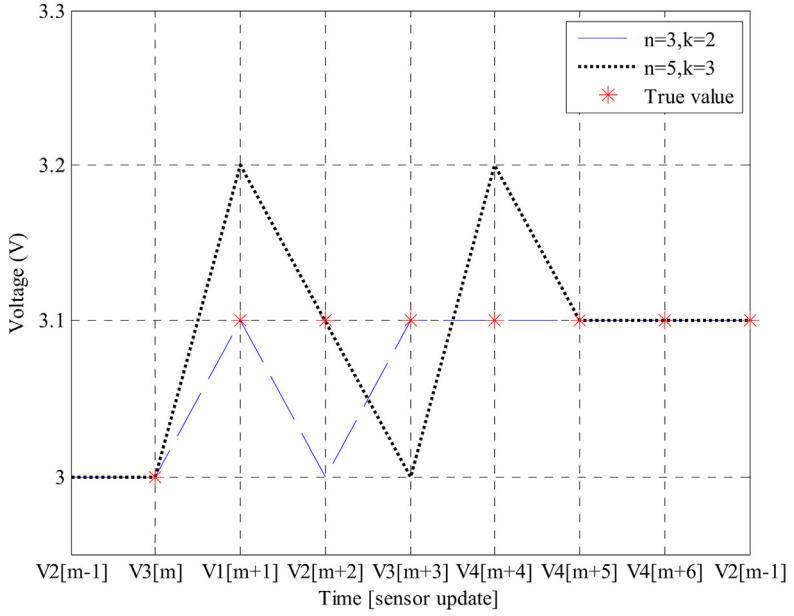

(a) Voltage ripples are found in sequential measurement.

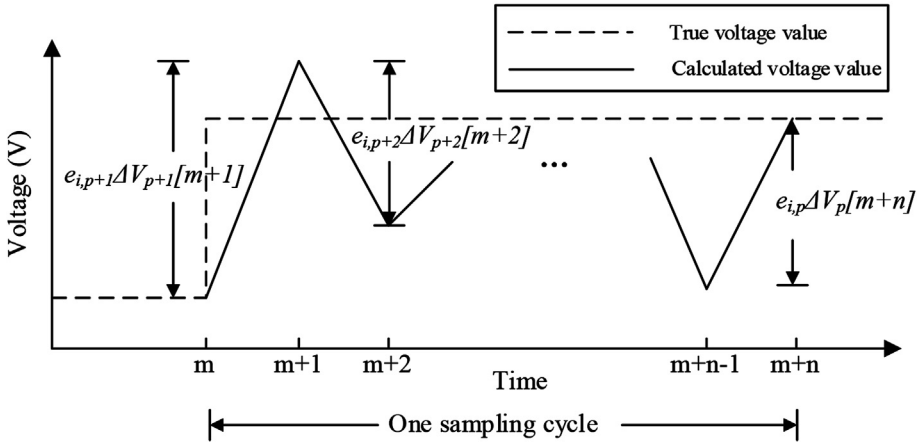

(b) The general sequential update process.

Fig. 8. The impact of sequential measurement on battery voltages.

The simulation result shows that it takes a whole sampling cycle to update every sensor measurement, and the voltage ripples appear during the update process. The general update process is illustrated in Fig. 8(b) qualitatively. Since the final terminal voltage settles at the right value, all the voltage ripples add up to the voltage step increase, i.e,

$$C_i[m+n] = C_i[m] + \sum_{j=1}^{n} e_{i,ind(p+j,n)} \Big\{ V_{ind(p+j,n)}[m+j] - V_{ind(p+j,n)}[m+j-n] \Big\} \quad (22)$$

where *ind(p + j,n)* is the rotating sensor index,

$$ind(x,n) = \begin{cases} n & , \ rem(x,n) = 0 \\ rem(x,n) & , \ otherwise \end{cases} \quad (23)$$

where *rem(x,n)* is the remainder of $\frac{x}{n}$.

Equation (22) shows that sensor $p + 1$ senses the voltage step increase first and each succeeding voltage sensors is updated one per time step, until sensor p is updated and the cell voltage converges to the right value. The whole process takes n time steps, which equal one full sampling cycle.

It can be found that these voltage ripples increase measurement noise significantly. As expected from Fig. 8(b), the noise is proportional to the $\frac{k-1}{k}$ times voltage change in sensors and thus increases linearly with $k-1$. Given 100 mV instant terminal voltage change for one cell in dynamic operations, the sequential measurement will lead to 100 mV measurement error for $n = 5$ and $k = 3$, which is not desirable.

The other impact of the sequential measurement is on fault detection and isolation. Since all the voltage sensors are updated sequentially, the fault signals becomes a time series of signals. For example, as the case of Fig. 2(a), the sensor voltages will not all change at 300 s. Due to sequential sensor updates, the change of V_3 will lag that of V_2 for one time step. With this impact, the fault detection and isolation need to be adapted from examining signal changes at one time to examining signal changes within a sampling period. In addition, as discussed in section 2.1, the voltage change in one sensor reading is regarded as sensor fault, which is always the case in sequential measurements. Therefore the extension of the proposed method to sequential measurement requires much more work in signal processing, more memory space and more computation.

6.4.3. Conversion of sequential measurement to simultaneous measurement

Given the limitation in the extension of the proposed topology to sequential measurement, a conversion methodology is provided to modify sequential measurement to simultaneous measurement in practical application.

Assume a battery module consists of M cells in series, and N modules form a whole pack. Within one module, a set of sequential measurement circuit is used to measure the voltages. Thus, a total N ADC channels and N measurement circuits are utilized.

In the traditional arrangement, the cell voltage is updated sequentially within one module, which leads to undesired sequential update.

The traditional arrangement can be modified by the following procedure.

1) The NM cells in the pack are regrouped into M new modules with N cells in each module.
2) For one time step, all the N ADC channels are used to measure the cell voltages within one module, and the cell voltages in other modules are updated sequentially.

In this way, the sequential cell voltage measurement in traditional topology is adapted to its equivalent simultaneous cell voltage measurement topology, with module voltage sequentially updated.

6.5. Condition for valid measurement topology

Not all combinations of n's and k's give valid **A** matrices. In some cases, the constructed **A** matrix is not invertible and thus the cell voltages cannot be obtained from sensor readings. One of the examples is $n = 6$ and $k = 2$. In order to increase the adaptability of the method, it is necessary to investigate the condition that gives invertible **A** matrices.

The **A** matrix can be formulated mathematically as follows,

a) **A** is an $n \times n$ matrix.
b) The first row consists of k consecutive '1's followed by $(n-k)$ consecutive '0's, $2 \le k < n$.
c) The m^{th} row is obtained by rotating every entry of the $(m-1)^{th}$ row to right by one position, and put the last entry of the $(m-1)^{th}$ row to the first entry of the mth row, $2 \le m \le n$.

An example **A** matrix with $n = 5$ and $k = 2$ is given in (4).

The final result is that n and k should be relatively prime, so that the associated **A** matrix is invertible. This statement is proved in two steps given below.

Step 1: If n and k are not relatively prime, the determinant of **A**, denoted as *det(A)*, is zero.

Assume $k = ae$, $n = be$, where $a < b$ and $a, b, e \in N$

If the m^{th} row of **A** is denoted as *row(m)*,

Thus $\sum_{m=0}^{b-1} row(1+me) = \sum_{m=0}^{b-1} row(2+me) = \ldots\ldots = \sum_{m=0}^{b-1} row(e+me)$

Hence $det(A) = 0$.

Step 2: If n and k are relatively prime, *det(A)* is nonzero.

A matrix can be written in the general form as shown as (24).

If each row is subtracted by its proceeding row, except the last row, without varying the determinant, **A** matrix is modified into (25).

The modified matrix is denoted as **B**, and its entries are denoted as $b_{i,j}$, where i is the row number and j is the column number.

Next, the Leibniz formula is applied to determine *det(A)*. The Leibniz formula expresses the determinant of square matrices with permutation of matrix entries [25], as (26).

$$\begin{array}{l} \\ row(1) \\ row(2) \\ \vdots \\ \vdots \\ row(n-k+1) \\ row(n-k+2) \\ \vdots \\ row(n) \\ \\ \end{array} \overset{\overset{k \text{ '1's}}{\overbrace{}}\ \overset{(n-k) \text{ '0's}}{\overbrace{}}}{\begin{bmatrix} 1 & \cdots & \cdots & 1 & 0 & \cdots & \cdots & 0 \\ 0 & 1 & \cdots & \cdots & 1 & 0 & \cdots & 0 \\ \vdots & \ddots & \ddots & & & \ddots & & \\ \vdots & & \ddots & \ddots & & & \ddots & \\ 0 & \cdots & \cdots & 0 & 1 & \cdots & \cdots & 1 \\ 1 & 0 & \cdots & \cdots & 0 & 1 & \cdots & 1 \\ \vdots & \ddots & \ddots & & & \ddots & \ddots & \vdots \\ 1 & \cdots & 1 & 0 & \cdots & \cdots & 0 & 1 \end{bmatrix}} \quad (24)$$

$$\underbrace{}_{(k-1) \text{ '1's}}\ \underbrace{}_{(n-k) \text{ '0's}}$$

$$\begin{array}{c} \\ row(1) \\ row(2) \\ \vdots \\ \vdots \\ row(n-k) \\ row(n-k+1) \\ \vdots \\ \vdots \\ row(n-1) \\ row(n) \end{array} \overset{\begin{array}{cccccccccc} \overbrace{\quad\quad\quad\quad\quad}^{k \text{ entries}} & & & & & \overbrace{\quad\quad\quad\quad\quad}^{(n-k) \text{ entries}} & & & & \end{array}}{\begin{bmatrix} 1 & 0 & \cdots & \cdots & 0 & -1 & 0 & \cdots & \cdots & 0 \\ 0 & 1 & 0 & \cdots & \cdots & 0 & -1 & 0 & \cdots & 0 \\ \vdots & \ddots & \ddots & \ddots & & & \ddots & \ddots & & \\ \vdots & & \ddots & \ddots & \ddots & & & \ddots & \ddots & \\ 0 & \cdots & \cdots & 0 & 1 & 0 & \cdots & \cdots & 0 & -1 \\ -1 & 0 & \cdots & \cdots & 0 & 1 & 0 & \cdots & \cdots & 0 \\ \vdots & \ddots & \ddots & & & \ddots & \ddots & \ddots & & \vdots \\ \vdots & & \ddots & \ddots & & & \ddots & \ddots & \ddots & \vdots \\ 0 & \cdots & 0 & -1 & 0 & \cdots & \cdots & 0 & 1 & 0 \\ 1 & \cdots & \cdots & 1 & 0 & \cdots & \cdots & \cdots & 0 & 1 \end{bmatrix}} \quad (25)$$

$$\begin{array}{cc} \underbrace{\quad\quad\quad}_{(k\text{-}1) \text{ '1's}} & \underbrace{\quad\quad\quad\quad}_{(n-k) \text{ '0's}} \end{array}$$

$$\det(A) = \sum_{\sigma \in S_n} \operatorname{sgn}(\sigma) \prod_{i=1}^{n} a_{i,\sigma(i)} \quad (26)$$

where S_n is the set of all permutations of 1,2, …,n, σ is one of the permutations within S_n. The $\operatorname{sgn}(\sigma)$ function is $+1$ for $\sigma = \sigma_0 = [1, 2, \ldots, n]$. If σ involves odd number of pairwise exchanges from σ_0, $\operatorname{sgn}(\sigma)$ is -1. If σ involves even number of pairwise exchanges from σ_0, $\operatorname{sgn}(\sigma)$ is $+1$.

Here lists two key facts of the Leibniz formula,

1) If $a_{i,j}$ is one of the terms in the product term $\prod_{i=1}^{n} a_{i,\sigma(i)}$, then any other entry in either row i or column j of **A** will not appear in the same product. In other words, in each of the product term, a row number or a column number should appear exactly once.
2) If any of the terms in one product is '0', then the whole product is zero.

It is important to note that there are $n!$ combinations of product terms for an $n \times n$ matrix if every product is taken into consideration. However, if the **B** matrix is treated, the many '0's are of great help to simplify the problem, since any product term involves '0' will end up with zero. Thus only the products with all nonzero entries contributes to the final summation.

There are k nonzero entries in *row(n)*, including $b_{n,1}$, $b_{n,2}$, …, $b_{n,k-1}$, and $b_{n,n}$. The following steps demonstrate a procedure to find the products with all nonzero entries. All of the products start from a term in *row(n)*.

1) $b_{n,n}$ is picked to form the first product. Thus no other entries from *row(n)* or *column(n)* can be picked in the same product term. It needs to be noted that there are only two terms in each row except *row(n)* in **B.** The choice of $b_{n,n}$ leaves only one choice of *row(n−k)*, because the '−1' in *row(n−k)* is in *column(n)*, thus $b_{n-k,n-k}$ has to be picked in the same product term, otherwise no entry from *row(n−k)* can be picked. If the remainder of $\frac{n-2k}{n}$ is expressed as *rem(n−2k,n)*, the choice of $b_{n-k,n-k}$ blocks the '−1' in *row(rem(n−2k,n))*, and $b_{rem(n-2k,n)\ rem(n-2k,n)}$ has to be picked. According to the proof given in Appendix B, if n and k are relatively prime, *rem(n−mk,n)* covers all the integers *1,2,3, …,n−1* for *m = 1,2,3, …,n−1*. It indicates that,
   i) All the row numbers and column numbers appears exactly once.
   ii) All the '−1's do not appear in the first product starting with $b_{n,n}$.
   iii) All the '1's along the diagonal of **B** have to be chosen in the first product starting with $b_{n,n}$.

   Hence, the first product is $b_{1,1}\, b_{2,2}\, b_{3,3} \ldots b_{n,n}$. The $\operatorname{sgn}(\sigma)$ function is evaluated as '1'. The product starting with $b_{n,n}$ is 1.

2) Since $k \geq 2$, $b_{n,1}$ should be '1'. In this step, $b_{n,1}$ is picked as the term from *row(n)* to form the second product. Clearly, $b_{n,1}$ blocks '1' from *row(1)* and '−1' from *row(n−k + 1)*. In this case, $b_{1,1+k}$ and $b_{n-k+1,n-k+1}$ has to be chosen in the second product. The procedure how every term in the product is chosen is given in (27).

$$b_{n,1} \Rightarrow \begin{cases} b_{1,1+k} & \Rightarrow b_{1+k,rem(1+2k,n)} & \Rightarrow \ldots \Rightarrow b_{n-k,n} \\ b_{rem(1-k,n),rem(1-k,n)} & \Rightarrow b_{rem(1-2k,n),rem(1-2k,n)} & \Rightarrow \ldots \Rightarrow b_{k,k} \end{cases} \quad (27)$$

The off-diagonal terms in the second product are '−1's, except $b_{n,1}$ is '1'. The choice of all the '−1's can be viewed as changing some of entry choices of the first product obtained in step 1, as shown in Table 2.

The row index of step 1) terms and step 2) terms in Table 2 are the same. If there are p terms different between step 2) and step 1), there are $(p-1)$ terms involved in the '1' to '−1' shift (exclude $b_{n,n}$ to $b_{n,1}$). The pairwise exchange number of the column indices from step 1) to step 2) is $(p-1)$. Since all the other diagonal terms remains to be '1', the product in step 2) is $\operatorname{sgn}(\sigma_{p-1})(-1)^{p-1}$. If $p-1$ is even, $\operatorname{sgn}(\sigma_{p-1}) = 1$, $(-1)^{p-1} = 1$, the product is 1. If $p-1$ is odd, $\operatorname{sgn}(\sigma_{p-1}) = -1$, $(-1)^{p-1} = -1$, the product is also 1.

Hence the product starting with $b_{n,1}$ is 1.

3) When $k > 2$, the procedure in step 2) can be generalized to products starting with $b_{n,q}$, where $2 \leq q \leq k$. The procedure how each product multiply is chosen is given in (28),

$$b_{n,q} \Rightarrow \begin{cases} b_{q,q+k} & \Rightarrow b_{rem(q+k,n),rem(q+2k,n)} & \Rightarrow \ldots \Rightarrow b_{n-k,n} \\ b_{rem(q-k,n),rem(q-k,n)} & \Rightarrow b_{rem(q-2k,n),rem(q-2k,n)} & \Rightarrow \ldots \Rightarrow b_{k,k} \end{cases} \quad (28)$$

Similarly, all the diagonal terms are '1's, and all the off-diagonal terms are '−1's except $b_{n,q}$. It needs to be noted that, in the analysis

Table 2
Relation between the choices in step 1) and step 2).

Off-diagonal terms in step 2)	Value	Corresponding terms in step 1)	Value
$b_{1,1+k}$	−1	$b_{1,1}$	1
$b_{1+k,rem(1+2k,n)}$	−1	$b_{1+k,1+k}$	1
⋮	−1	⋮	1
$b_{n-k,n}$	−1	$b_{n-k,n-k}$	1
$b_{n,1}$	1	$b_{n,n}$	1

Table 4
Advantages and disadvantages of the proposed sensing topology.

Advantages	Disadvantages
Fully utilize duplicated components.	Lead to higher noise level.
Require no additional components.	Require higher sensor range.
Distinguish between sensor/cell faults.	

Table 3
Summary of results of changing n and k for $n \leq 16$ and $k \leq 4$.

	n	k
Increase	Increase noise.	Increase confidence level in fault detection. Increase noise.
Decrease	Limit maximum value of k.	Lower voltage measurement range, lower hardware cost.

of step 2, whether the number 'p' is odd or even does not affect the evaluation of $\mathrm{sgn}(\sigma)$ function. Hence, the products starting with any $b_{n,q}$ is 1, when $2 \leq q \leq k$.

4) At last, the Leibniz formula sums all the products. In the case of **B**, each of the '1's in *row(n)* leads to a product of 1. Therefore, $det(A) = det(B) = k$.

By now, it is clear that when n and k are not relatively prime, *det(A)* is zero, or **A** is noninvertible; when n and k are relatively prime, *det(A)* is nonzero, or **A** is invertible. Therefore, in order to obtain the battery cell voltages from voltage sensor measurements, only n's and k's that are relatively prime should be used to design the measurement topology.

6.6. Optimal choice of n and k

The optimal choice of n and k involves tradeoff among many factors. In the later discussion, $n \leq 16$ and $k \leq 4$ are assumed for practical application. The results are summarized in Table 3.

n: when n is increased, the number of cells that involves in a whole measurement group increases. Thus the noise levels of the calculated cell voltage increases. When n is decreased, since $k < n$, the maximum value of k is limited.

k: when k is increased, the number of cells one voltage sensor measures increases accordingly. This leads to higher measurement range for each of the voltage sensor, which further results into higher hardware cost and higher noise level. The benefit of increased k is that the *CL* of sensor fault detection is increased.

7. Conclusion

A fault-tolerant voltage measurement method is proposed for the BMS of electric vehicles with no extra sensor or software added. A matrix interpretation is developed to simultaneous sensor measurements. The analysis shows the viability of the proposed measurement topology in isolating cell failure and sensor failure by measuring the voltage sum of multiple battery cells. A modified electronic circuit is proposed to implement the proposed measurement topology. Through the use of this concept, the confidence of sensor failure and cell failure detection are greatly improved, while no additional cost is added to the system. Simulation and experiment results show that sensor and cell faults can be identified and isolated by locating the abnormal signals. The robustness of the method is tested by applying UDDS cycles to the cells and no false detection is induced by normal operation behavior.

Next, the voltage measurement method is generalized to n series connected cells with k consecutive voltage sum measurement. Reliability prediction analysis shows the increase of k will improve the fault detection confidence level. The application of probability theory indicates that the increase of n and k will increase noises levels in the calculated cell voltage values, whereas the decrease of n will limit the upper bound of k. Simulation shows that the application of the proposed method is limited in sequential measurements, however, with a proposed procedure, a sequential measurement topology can be always converted into an equivalent simultaneous measurement topology. Finally, the feature of valid measurement topology, i.e. the condition of n and k to construct invertible **A** matrix, is discovered by mathematical proof as that n and k need to be relatively prime.

The advantages and disadvantages of the proposed method is summarized in Table 4. This method fully utilizes duplicated components in the sensing circuit, and interleaves them to increase fault detection credibility. The major limitation of this method are 1) the range of the sensors are increased, then the cost will increase; 2) the noise is increased. It needs to be noted that this fault-tolerant measurement concept can also be further extended to other physical quantity measurements in which distinction between sensor faults and device faults is critical.

Acknowledgements

The authors would like to acknowledge Dr. Randy Stevenson, Ms. Yuhong Fu, and Ms. Minqian Zhang for their great discuss and help in the study.

Appendix A

Proof of statement: The inverse matrix of **A** has the feature that as the row number increases by one, the entries rotate to right by one position.

Proof: An **A** matrix is constructed for n cells and n voltage sensors, as shown in (A.1). The $\mathbf{A}^{-1}$ matrix is represented in (A.2).

A similar matrix representation can be constructed by rotating the entries of both **V** and **C**, as shown in (A.3). It needs to be noted that the **A** matrix does not change, and it is the same as that in (A.1). Hence, the $\mathbf{A^{-1}}$ in (A.4) is also the same as that in (A.2). This indicates that $C_1 = [row_{A^{-1}}(1)][V_1 \quad V_2 \quad \dots \quad V_{n-1} \quad V_n]^T$, and $C_2 = [row_{A^{-1}}(1)][V_2 \quad V_3 \quad \dots \quad V_n \quad V_1]^T$. If the sensor matrix of C_2 is changed from $[V_2 \quad V_3 \quad \dots \quad V_n \quad V_1]^T$ to $[V_1 \quad V_2 \quad \dots \quad V_{n-1} V_n]^T$, every entry of $row_{A^{-1}}(1)$ will need to be rotated to right by one position.

The same procedure can be applied to other cell values and the statement is proved.

$$\begin{bmatrix} V_1 \\ V_2 \\ \vdots \\ V_{n-1} \\ V_n \end{bmatrix} = \begin{bmatrix} row_A(1) \\ row_A(2) \\ \vdots \\ row_A(n-1) \\ row_A(n) \end{bmatrix} \begin{bmatrix} C_1 \\ C_2 \\ \vdots \\ C_{n-1} \\ C_n \end{bmatrix} \quad (A.1)$$

$$\begin{bmatrix} C_1 \\ C_2 \\ \vdots \\ C_{n-1} \\ C_n \end{bmatrix} = \begin{bmatrix} row_{A^{-1}}(1) \\ row_{A^{-1}}(2) \\ \vdots \\ row_{A^{-1}}(n-1) \\ row_{A^{-1}}(n) \end{bmatrix} \begin{bmatrix} V_1 \\ V_2 \\ \vdots \\ V_{n-1} \\ V_n \end{bmatrix} \quad (A.2)$$

$$\begin{bmatrix} V_2 \\ V_3 \\ \vdots \\ V_n \\ V_1 \end{bmatrix} = \begin{bmatrix} row_A(1) \\ row_A(2) \\ \vdots \\ row_A(n-1) \\ row_A(n) \end{bmatrix} \begin{bmatrix} C_2 \\ C_3 \\ \vdots \\ C_n \\ C_1 \end{bmatrix} \quad (A.3)$$

$$\begin{bmatrix} C_2 \\ C_3 \\ \vdots \\ C_n \\ C_1 \end{bmatrix} = \begin{bmatrix} row_{A^{-1}}(1) \\ row_{A^{-1}}(2) \\ \vdots \\ row_{A^{-1}}(n-1) \\ row_{A^{-1}}(n) \end{bmatrix} \begin{bmatrix} V_2 \\ V_3 \\ \vdots \\ V_n \\ V_1 \end{bmatrix} \quad (A.4)$$

Appendix B

Proof of statement: Given two positive integers that are relatively prime, a and b, $a < b$. The remainders of $\frac{ma}{b}$ covers all the integers *1,2, …,b−1*, for $m = 1,2, \ldots,b-1$.

Proof:

a and b are relatively prime, $m < b$

=> for $m = 1,2, \ldots,b-1$, every $\frac{ma}{b}$ has a remainder. (The least common multiple of a and b should be ba.)

In order to prove that every integer in *1,2, …,b−1* is covered by the remainders, it still needs to prove that any two of the *b−1* remainders do not have same value. Next, it is proved by contradiction.

Suppose: Two of the remainders are same.

It can be expressed as that the remainders of $\frac{xa}{b}$ and $\frac{ya}{b}$ are the same, $1 \le x < y \le b-1 \;\; x, y \in N$.

Then $(y-x)a = cb, c \ge 1, c \in N$

Thus $(y-x)a$ is a multiple of both a and b

However $y-x < b$

$\Rightarrow (y-x)a < ba$

$\Rightarrow ba$ is not least common multiple of a and b

$\Rightarrow a$ and b are not relatively prime

This is contradict to the condition that a and b are relatively prime.

Therefore the assumption is false, none of two remainders have the same value.

It indicates that the *b−1* remainders are different with one another and their range is $[1, b-1]$, so they covers every integer in that range.

References

[1] X. Zhang, C. Mi, Vehicle Power Management: Modeling, Control and Optimization, Springer Science & Business Media, 2011.
[2] T.G. Goonan, Lithium Use in Batteries, US Department of the Interior, US Geological Survey, 2012.
[3] D. Doughty, E.P. Roth, Electrochem. Soc. Interface 21 (2012) 37–44.
[4] N. Williard, W. He, C. Hendricks, M. Pecht, Energies 6 (2013) 4682–4695.
[5] Q. Wang, P. Ping, X. Zhao, G. Chu, J. Sun, C. Chen, J. Power Sources 208 (2012) 210–224.
[6] F. Thomas, G. Mills, R. Howe, J. Zobell, Air Med. J. 31 (2012) 242–248.
[7] X. Feng, M. Fang, X. He, M. Ouyang, L. Lu, H. Wang, M. Zhang, J. Power Sources 255 (2014) 294–301.
[8] J. Anderson, F. Larsson, P. Andersson, B.-E. Mellander, in: Fires in Vehicles (FIVE) 2014 Conference Proceedings, 2014, pp. 267–270.
[9] L. Lu, X. Han, J. Li, J. Hua, M. Ouyang, J. Power Sources 226 (2013) 272–288.
[10] M. Brandl, H. Gall, M. Wenger, V. Lorentz, M. Giegerich, F. Baronti, G. Fantechi, L. Fanucci, R. Roncella, R. Saletti, in: Proceedings of the Conference on Design, Automation and Test in Europe, EDA Consortium, 2012, pp. 971–976.
[11] G.-H. Kim, K. Smith, J. Ireland, A. Pesaran, J. Power Sources 210 (2012) 243–253.
[12] X. Bing, C. Mi, C. Zheng, B. Robert, in: Transportation Electrification Conference and Expo (ITEC), 2015 IEEE, 2015, pp. 1–7.
[13] B. Xia, Z. Chen, C. Mi, B. Robert, in: Transportation Electrification Conference and Expo (ITEC), 2014 IEEE, IEEE, 2014, pp. 1–7.
[14] C.-H. Kim, M.-Y. Kim, G.-W. Moon, Power electronics, IEEE Trans. 28 (2013) 3779–3787.
[15] L. Technology, Multicell Battery Monitors, 2015, Nov 13. Available, http://cds.linear.com/docs/en/datasheet/680412fb.pdf.
[16] Panasonic, Battery Voltage Measurement IC, 2015, Nov 13. Available, http://www.semicon.panasonic.co.jp/en/news/contents/2013/embeddedworld/flyer/BMS_IC_EW13.pdf.
[17] C.-L. Chen, D.-S. Wang, J.-J. Li, C.-C. Wang, Very large scale integration (VLSI) systems, IEEE Trans. 23 (2015) 244–253.
[18] V.P. Nelson, Computer 23 (1990) 19–25.
[19] G.H.B. Foo, X. Zhang, D.M. Vilathgamuwa, Industrial electronics, IEEE Trans. 60 (2013) 3485–3495.
[20] I. Hwang, S. Kim, Y. Kim, C.E. Seah, Control systems technology, IEEE Trans. 18 (2010) 636–653.
[21] M. Rausand, A. Høyland, System Reliability Theory: Models, Statistical Methods, and Applications, John Wiley & Sons, 2004.
[22] P. O'Connor, A. Kleyner, Practical Reliability Engineering, John Wiley & Sons, 2011.
[23] R.B. Ash, Basic Probability Theory, Courier Corporation, 2012.
[24] S.W. Smith, Digital Signal Processing: a Practical Guide for Engineers and Scientists, Newnes, 2003.
[25] M. Fluch, in, Department of Mathematics ans Statistics, University of Helsinki, 2007.